

*Chapter 8*

## **A MOBILE HAPTIC INTERFACE FOR BIMANUAL MANIPULATIONS IN EXTENDED REMOTE/VIRTUAL ENVIRONMENTS**

*Angelika Peer*\*, *Thomas Schauß*†,  
*Ulrich Unterhinninghofen*‡, and *Martin Buss*§  
Institute of Automatic Control Engineering  
Technische Universität München

### **Abstract**

The concept of a new mobile haptic interface for unconstrained bimanual manipulation is presented. This device, which has been developed at the High-Fidelity Telepresence and Teleaction Research Centre, Munich, Germany, allows locomotion and haptic interaction at the same time. In contrast to most existing haptic interfaces, it is therefore not restricted to desktop applications but also enables bimanual manipulation tasks with high interaction forces in extended remote or virtual environments. The design of this mobile haptic interface is based on a modular system consisting of two components: two haptic interfaces and a mobile platform. While the haptic interfaces only cover parts of the human arm workspace, the mobile platform extends these to arbitrarily large remote environments. A special design and control concept of the haptic interfaces makes it possible to decouple translational from rotational movements. This decoupling helps to significantly simplify the control algorithms which handle the interaction between the single components. The mobile platform which carries the two haptic interfaces must be positioned in such a way that the manipulability of both haptic interfaces is maximized. Different optimization strategies are presented and compared. The motion of the mobile platform must be synchronized with the control of the haptic interfaces in order to hide the platform motion from the operator. Finally, experimental results are presented.

---

\*E-mail address: angelika.peer@tum.de

†E-mail address: thomas.schauss@mytum.de

‡E-mail address: ulrich.unterhinninghofen@tum.de

§E-mail address: mb@tum.de

## 1. Introduction

Haptic interfaces can be described as bidirectional human-system-interfaces. On the one hand they provide the operator with force/torque information from virtual or remote environments and on the other hand they are used to read the motion/force input of the operator. In recent years haptic devices have received a lot of attention: They found their way into applications such as medical training, rehabilitation, virtual prototyping, telesurgery, tele-maintenance as well as micromanipulation.

However most existing haptic interfaces are limited in their degrees of freedom (d.o.f.), have only a small workspace or/and a low output capability (velocity, acceleration, and force/torque capability). Thus tasks which require 6 d.o.f. manipulations with high interaction forces (high output capability) in extended remote or virtual environments (big workspace) are not possible.

In order to overcome these limitations, a concept for a new mobile haptic interface has been developed. The mobile haptic interface consists of two different main components: two haptic interfaces and a mobile platform. While the haptic interfaces only cover parts of the human arm workspace, the mobile platform extends these to arbitrarily large remote environments.

Possible applications for such a system are e.g. the control of a mobile teleoperator in a telepresence scenario or the haptic exploration in extended virtual environments as e.g. a virtual museum, see Fig. 1.

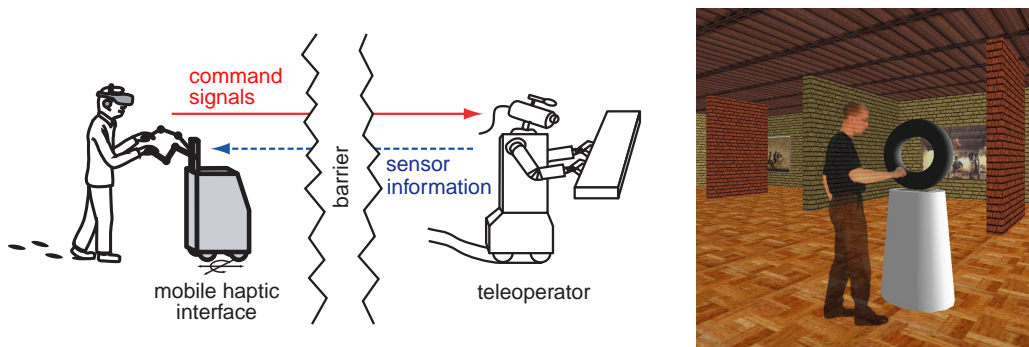


Figure 1. Application scenarios of a mobile haptic interface: teleoperation system (left), exploration of a virtual museum (right)

This paper is structured as follows: The following Section 2. starts with a review of the state of the art in the field of stationary and mobile haptic devices. This section will be followed by a design rationale and description of the new mobile haptic interface. Section 4. presents different control algorithms which have been applied to the new device and Section 5. reports some experimental validation results. Finally, Section 6. concludes the paper and shows directions of future research.

## 2. State of the Art

In the past years, the interest in the development of haptic devices for telerobotic applications has dramatically increased. A huge number of different kinds of haptic devices has been developed and partly commercialized. But almost all of these devices are stationary devices with quite a small workspace and a moderate force level. In order to increase the workspace of such devices, usually hand controlled input devices such as a joystick or mouse are used [8] or some indexing technique is applied. If control by the operator's hand is not possible, as in the case of bimanual manipulation, these devices can also be substituted by a special kind of foot pedal [2, 14].

Since the operator can not move around, none of these approaches provide a proprioceptive perception of locomotion. As shown in [3], such incomplete or false proprioceptive cues result in a deterioration of the natural orientation and navigation capabilities of a human operator.

More realistic locomotion interfaces such as treadmills and tracking systems for human operator locomotion can be found in the field of virtual reality applications. These systems allow the human operator to freely move around in the remote environment but do not provide any force feedback information. Thus, simultaneous manipulation and locomotion is not possible.

A known approach to circumvent this problem and allow simultaneous manipulation and locomotion is to use body grounded haptic interfaces such as exoskeletons. But as reported in [16], working with exoskeletons is very fatiguing since the range of human arm movements is restricted and/or long time operations are not possible because of the high weight of the system. In addition, mounting application specific end-effectors is extremely difficult.

A much more advanced locomotion interface has been proposed in [10, 11] and later adapted in [4]. They mounted a stationary haptic interface on a mobile platform. Since in this case the weight of the haptic interface is fully supported by the platform, the operator fatigue can be significantly reduced. But these systems allow only one-handed manipulation and their haptic interfaces are limited to either 3 or 4 d.o.f. In [12] the first bimanual mobile haptic interface for haptic grasping in large virtual environments was presented, but again haptic interfaces with only 3 d.o.f. were used.

The research presented here focuses on the development of a bimanual mobile haptic interface with the ability to manipulate in full 6 d.o.f. Since the design is based on two independently controlled modules - mobile platform and haptic interfaces - haptic interfaces with at least 6 d.o.f. are required. In addition a high output capability and bandwidth is necessary to represent stiff environments.

Stationary haptic interfaces that achieved a sufficient development status are mostly characterized by highly lightweight mechanical designs requiring no active force feedback control to provide a good backdrivability. E.g. the PHANToM family [9] belongs to that kind of systems. Only a few devices, e.g. the PHANToM Premium as well as the DELTA Haptic Device [5] show an improved but still moderate output capability. As the device workspace and therefore also the device size increase force sensing is necessary to compensate for the increased friction and inertia. The HapticMASTER [20] is an example for such a haptic device which provides 100 N continuous force, but is limited to 3 d.o.f. The

6 d.o.f. device Mirage F3D-35 Haptic System [15] satisfies the force requirements (peak forces of about 100 N), but is limited to a quite small workspace. The most advanced haptic interfaces are the Virtuose 6D40-40 with 30 N continuous force and a workspace of the human arm reach as well as the INCA 6D of Haption with 40 N continuous force and an almost unlimited operational workspace. While the former is too bulky to be mounted on a mobile platform, which is necessary for unconstrained bimanual manipulation, the latter seems to be only suitable for one handed operations.

In order to fill this gap a new bimanual admittance type haptic interface called ViSHARD7 has been developed, which is mountable on a mobile platform. Thus it is not restricted only to desktop applications but also enables bimanual manipulation tasks with high interaction forces in extended remote or virtual environments.

### 3. System Setup

The mobile haptic interface comprises two haptic interfaces with seven degrees of freedom (ViSHARD7) each covering the most important working range of the human arm. These two haptic interfaces are mounted on a mobile platform which extends the usable workspace to arbitrarily large environments. Using this setup, the operator can freely move around in the virtual or remote environment and interact with it at the same time. An overview of the complete system is shown in Fig. 2. It represents a typical application scenario where the operator is immersed in a remote or virtual environment by wearing a head mounted display (HMD). This section provides a description of the single components, haptic interfaces and mobile platform, and specifies their connections.

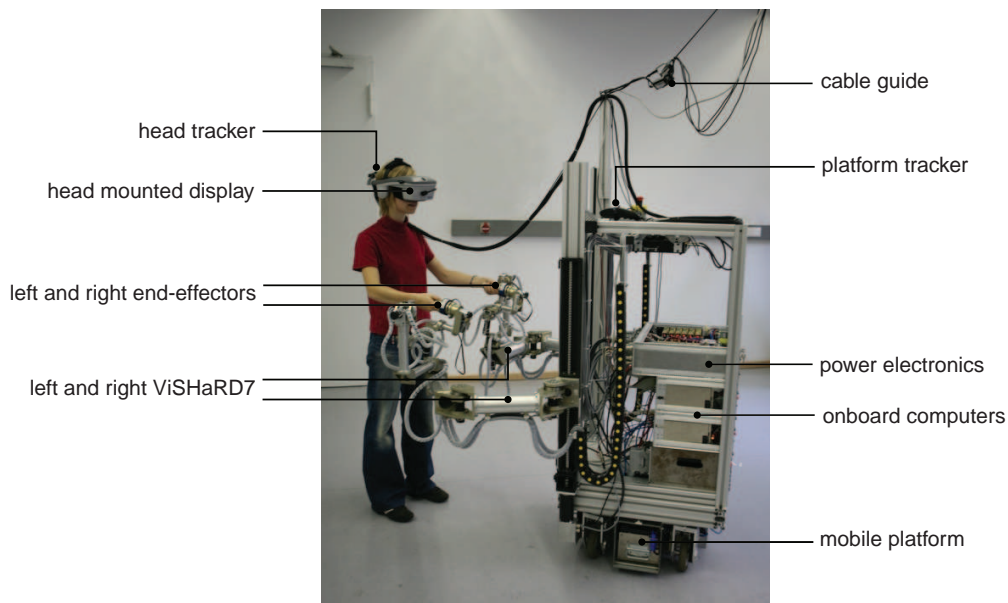


Figure 2. Hardware setup in a typical application scenario.

### 3.1. Haptic Interfaces

The kinematic structure of one of the haptic interfaces, called VISHARD7 (Virtual Scenario Haptic Rendering Device with 7 actuated d.o.f.), is illustrated in Fig. 3. It shows the reference configuration with all joint angles  $q_i$  defined to be zero. The corresponding link length design is summarised in Tab. 1. Fig. 4 shows a typical operational configuration.

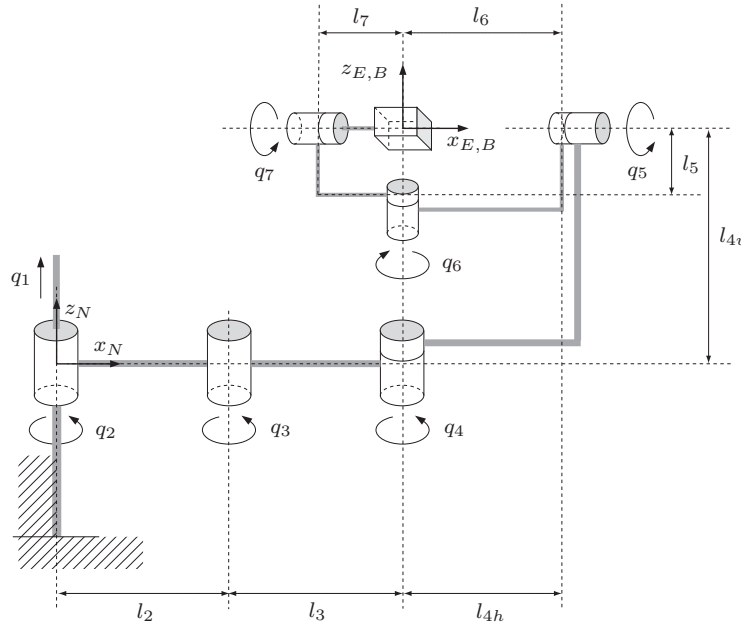


Figure 3. Kinematic model of VISHARD7.

The first joint has been designed as linear axis and enables vertical motions in  $z_N$ -direction. Joint 2 and 3 are arranged in a SCARA configuration and allow positioning in the  $x_N$ - $y_N$  plane. As known in the literature, the maximum manipulability of such a two-link planar arm can be achieved for a construction with equal joint lengths. Thus, the link lengths two and three have been set to  $l_2 = l_3 = 0.35$  m.

The SCARA part is in a singular configuration when link 2 and 3 are collinear. Hence, configurations near the base have to be omitted. Joint 4 is used to prevent singular configurations in the wrist formed by joints 5, 6, and 7. Singularities in the wrist arise when the axes of joint 5 and 7 are collinear, which can be avoided by a rotation of joint 4. An adequate inverse kinematics algorithm guarantees singularity free operation.

VISHARD7 has been designed in such a way that joint 4, 5, 6, 7 intersect in a single point, where the angular d.o.f. are mechanically decoupled from the translational ones. As already mentioned in [19], such a mechanical decoupling of the angular from the translational d.o.f. has several advantages: The natural dynamics of the orientational d.o.f. is reduced and the torque capability of the rotational actuators can be chosen to match the capability of a human wrist so that no additional safety mechanisms are required. In the case of designing a mobile haptic interface consisting of two independently working components (haptic interface and mobile platform) such a construction can furthermore significantly simplify the algorithms which take care of the interaction between these two components.



**Table 1.** Link length design of VISHARD7

Link $i$	Length
$l_1$	0.6 m
$l_2 = l_3$	0.35 m
$l_{4h} = l_6$	0.2155 m
$l_{4v}$	0.3411 m
$l_5$	0.082 m
$l_7$	0.0654 m

Figure 4. Typical operational configuration.

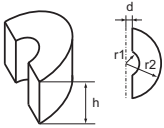
The link length design guarantees a reachable workspace of almost a half cylinder with radius and height of 0.7 m. Thereby, possible collisions with the arm itself and the platform are considered. In contrast to this reachable workspace, the specifications of the dextrous workspace of the device are given in Table 2.

The actuation torque of all rotational joints is provided by DC-motors coupled with harmonic drive gears offering zero backlash. For the linear axis, a *LM Guide Actuator* of THK has been chosen, which guarantees high rigidity and high accuracy. A brushless DC-motor, which carries the whole weight of all movable parts, is used to drive this linear axis. Since brushless DC-motors usually have better thermal properties than comparable DC-motors this results in a more compact design. An additional brake holds the haptic interface in a fixed position when no motor currents are provided. While all DC-motors of the rotational joints are supplied by Copley amplifiers configured in torque mode, the brushless DC-motor is driven by a 4QEC servo amplifier DES 70/10 of maxon motor with sinusoidal commutation and digital current control.

In order to permit force feedback control, the device is equipped with a six-axis JR3 force-torque sensor providing a bandwidth of 8 kHz at a comparatively low noise level. The joint angles of the rotational joints are measured by digital MR-encoders with a resolution of 4,096 counts per revolution, resulting in a high position resolution when multiplied with the gear ratio. The position of the linear axis is measured at the drive end by using a Scancon Encoder with a resolution of 30,000 counts per revolution (quadrature encoder). The combination of a slope of 10 mm/round of the linear axis and a maximum motor speed of 5,370 rpm allows translational velocities of up to 0.895 m/s. The maximum payload of the linear axis is 340 N and can be calculated considering the limit of the average torque of the motor, the slope of the linear axis, and the mass of all moving parts.

Matlab/Simulink Real-Time-Workshop is used to automatically generate code from Simulink models, which is then executed on a RTAI real time operating system. All models run with a sampling rate of 1 kHz. Data acquisition is performed by using Sensoray S626 PCI-I/O boards.

**Table 2. Target specifications of VISHARD7**

Property	Value
transl. workspace	$h = 0.6 \text{ m}$ $d = 0.1 \text{ m}$ $r_1 = 0.2 \text{ m}$ $r_2 = 0.6 \text{ m}$ 
rot. workspace*	pitch, roll: $\pm 360^\circ$ yaw: $\pm 60^\circ$
peak force	vertical: 533 N horizontal: 155 N
peak torque	pitch, yaw: 11 Nm roll: 4.8 Nm
trans. velocity	vertical: 0.895 m/s horizontal: 1.1 m/s
rot. velocity*	pitch, yaw: 4.3 rad/s roll: 8.9 rad/s
trans. acceleration	vertical: $9.2 \text{ m/s}^2$ horizontal: $13.5 \text{ m/s}^2$
rot. acceleration*	pitch, yaw: $183 \text{ rad/s}^2$ roll: $318 \text{ rad/s}^2$
maximum payload**	34 kg
mass of moving parts	$\approx 13 \text{ kg}$

\* numbers refer to a device controlled by inverse function, see Sec. 4.1.1.

\*\* calculated for zero steady state human operator input force

### 3.2. Mobile Platform

The mobile platform of the mobile haptic interface is used to position the haptic interfaces in such a way that their workspace is not exceeded. Therefore, the mobile platform must follow the motions of the human operator. Consequently, it must be able to move in any direction and turn around its own axis. An omnidirectional mobile platform is used to fulfill these requirements.

An omnidirectional, holonomic platform offers the highest degree of maneuverability. Most holonomic platforms are based on Omni-Wheels or Meccanum-Wheels. In principle these wheels consist of small rollers or cones mounted on the circumference of a larger wheel. This allows the wheels to be driven like a standard wheel but it also allows sideways movements with low friction. With a proper wheel arrangement, true omnidirectional, holonomic behavior can be achieved. The disadvantage, however, is that the irregularities in the shape result in noise and vibrations during platform motions. These vibrations are very distracting in a device designed for haptic interaction.

An alternative design consists in using a platform with four conventional wheels which

can be independently driven and steered. This also allows omnidirectional maneuvering with low vibrations but at the cost of non-holonomic constraints. In order to realize abrupt changes of the driving direction the wheels need to be turned in the new direction. This can lead to delays in the realization of a given desired trajectory. However, in the given application, small deviations from the desired trajectory can be compensated by the haptic interfaces.

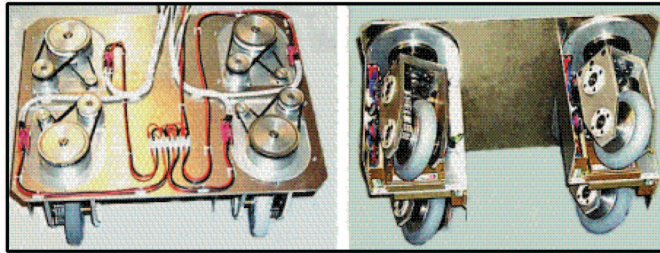


Figure 5. Hardware setup of mobile platform without payload

Following the above outlined rationale, an omnidirectional platform based on four conventional, independently driven and steered wheels is employed as base for the mobile haptic interface (see Fig. 5). The developed platform has a maximum payload of about 200 kg. Maximum speed is around 1.5 m/s, maximum driving power is 600 W. For further details on the mechanical design, the reader is referred to [6].

## 4. Control Design

The objective of the presented mobile haptic interface is to allow haptic interaction and locomotion at the same time. These two requirements can be attributed to the two different hardware components haptic interfaces ViSHaRD7 and omnidirectional mobile platform, respectively. As the dynamic properties of haptic interfaces and mobile platform differ significantly, their motions can be regarded as decoupled. Thus, the rendering of the desired environment admittance is solely performed by the haptic interfaces. In this section the control algorithms of the two different components - haptic interfaces and mobile platform - are presented and the coordination between them is discussed.

### 4.1. Control of ViSHaRD7

Realization of a human haptic interaction with a remote environment requires controlling of the motion-force relation between the operator and the haptic interfaces. This can be achieved by either controlling the interaction force of the device with the operator (impedance display mode) or the device motion (admittance display mode).

In order to provide effective compensation of the disturbances due to friction and the natural device dynamics, an admittance control strategy has been implemented for ViSHaRD7. In contrast to impedance control, which is frequently used for light and highly

backdrivable devices, admittance control is particularly well suited for robots with high dynamics and non-linearities. The high gain inner control loop closed on motion allows for an effective elimination of the nonlinear device dynamics. Interested readers may have a look at [17] for a more detailed analysis of haptic control schemes.

In admittance control the minimum target mass and inertia of the haptic display is bounded by stability: When the human operator touches the device and free space motion should be rendered, the device needs to accelerate very quickly. This again implies very high control gains, which cause potential stability problems during free space motion. Thus in free space motion a minimum mass and inertia necessary for stability of the master control have to be implemented. While the minimum mass is realized in form of a double integrator

$$\mathbf{f}_N = \mathbf{M}_T \ddot{\mathbf{x}}_N, \quad (1)$$

the implementation of the minimum rotational inertia  $\mathbf{M}_R$  is based on the well known Euler's dynamical equations of rotation, see [13] for more details. This master dynamics relates the interaction force  $\mathbf{F}_{\text{ext}}$  to the reference end-effector velocity  $\dot{\mathbf{x}}_r$ . An algorithm for inverse kinematics resolution calculates the reference joint velocities  $\dot{\mathbf{q}}_r$ . The joint angles  $\mathbf{q}_r$  finally are the reference input to a conventional position control law, e.g. independent joint controllers or a computed torque scheme.

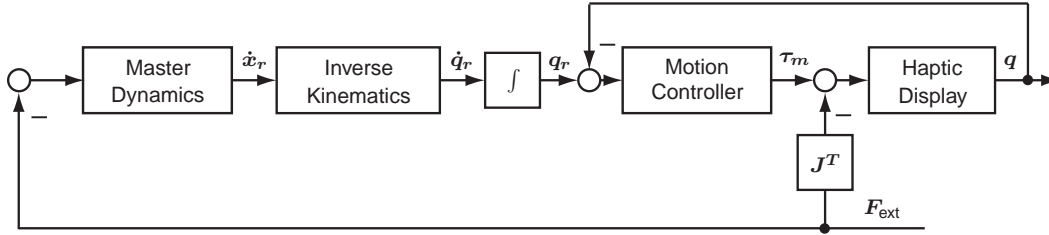


Figure 6. Admittance control scheme.

#### 4.1.1. Inverse Kinematics

The inverse kinematics, the mapping of the end-effector to the joint motion, can be either realized on the position

$$\mathbf{q} = \mathbf{f}(\mathbf{x}) \quad (2)$$

or on the velocity level.

$$\dot{\mathbf{q}} = \mathbf{f}(\dot{\mathbf{x}}), \quad (3)$$

whereby  $\mathbf{q}, \dot{\mathbf{q}} \in \mathbf{R}^n$  are the joint angle and velocity and  $\mathbf{x}, \dot{\mathbf{x}} \in \mathbf{R}^m$  the end-effector position and velocity. Since for VISHARD7  $n > m$  the manipulator is redundant with respect to the end-effector task. This redundancy allows changing the internal configuration without changing the position and orientation of the end-effector. This implies that no unique solution for the inverse kinematics problem given by (2) and (3) can be derived.

To solve this problem for the haptic input device VISHARD7 a simple inverse function for the whole haptic interface has been defined, which decouples translational from rotational movements and thus simplifies the interaction with the mobile platform.

A simple inverse function is defined when using the following mapping from joint angles to Cartesian positions:

$$q_1 = \left( \frac{2\pi}{0.01} \right) z, \quad (4)$$

$$q_2 = \arctan 2(y, x) + \cos^{-1} \left( \frac{x^2 + y^2}{2l\sqrt{x^2 + y^2}} \right), \quad (5)$$

$$q_3 = \cos^{-1} \left( 1 - \frac{x^2 + y^2}{2l^2} \right) + \pi, \quad (6)$$

where  $(x, y, z)$  is the end-effector position with respect to the haptic interface base coordinate system  $S_N$ ,  $q_i$  are the joint angles of the  $i$ -th joint, and  $l$  is the link length of link 2 and 3. By setting joint angle 4 to  $q_4 = q_{4,0} - \sum_{i=2}^3 q_i$ , a decoupling of translational and rotational motions can be achieved. It should be noted that this special inverse function implies a singular configuration at the point  $x = y = 0$ , which has to be omitted.

For the rotational part an inverse kinematics solution operating at the angular velocity level has been applied. In a first step the time derivative of the end-effector orientation (given by means of  $yzx$ -Euler-angles  $[\alpha, \beta, \gamma]$ ) can be calculated from the angular velocity of the end-effector  $\omega_B$ :

$$\begin{pmatrix} \dot{\alpha} \\ \dot{\beta} \\ \dot{\gamma} \end{pmatrix} = \begin{pmatrix} 0 & \frac{\cos \gamma}{\cos \beta} & -\frac{\sin \gamma}{\cos \beta} \\ 0 & \sin \gamma & \cos \gamma \\ 1 & -\frac{\sin \beta \cos \gamma}{\cos \beta} & \frac{\sin \beta \sin \gamma}{\cos \beta} \end{pmatrix} \omega_B. \quad (7)$$

Choosing the Euler-angles in such a way that they correspond to the joint angles  $q_5, q_6$  and  $q_7$  the inverse function for the rotational part is given with:

$$q_5 = \alpha, \quad (8)$$

$$q_6 = -\beta + \pi/2, \quad (9)$$

$$q_7 = \gamma. \quad (10)$$

This inverse kinematics solution has a singular configuration for  $\beta = k\pi/2$  with  $k \in \mathbb{N}$ , which however can be easily avoided by introducing a joint limitation for  $q_6$ .

## 4.2. Control of the Mobile Platform

The mobile platform is operated in velocity control mode. As the operator motions cannot be reliably predicted, a control scheme which does not rely on a preplanned path is used.

The kinematic structure of the mobile platform is depicted in Fig. 7a. The controller of the mobile platform needs to ensure the coordinated motion of all wheels, i.e. all wheel normals must be either parallel or intersect in a single point. The respective wheel configurations are called admissible wheel configurations (AWC). All AWCs can be represented on the surface of a unit sphere and can be described by using two spherical angles: the azimuth angle  $\eta$  represents the direction of the translational motion and the altitude  $\zeta$  is a measure for the relative amount of rotational motion. In Fig. 7b the unit sphere model is illustrated. All configurations on the equator ( $\zeta = 0$ ) correspond to pure translational motion

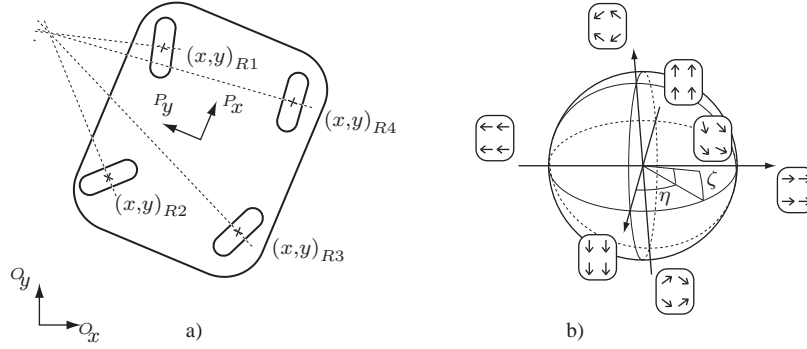


Figure 7. (a) Kinematic model of the mobile platform (b) Unit sphere representation of wheel configurations.

while configurations at one of the poles ( $\zeta = \pm\pi/2$ ) represent pure rotational motion. The absolute motion speed is described by a generalized velocity  $\omega$ .

A desired velocity in Cartesian coordinates  $\dot{\mathbf{x}} = (\dot{x}, \dot{y}, \dot{\psi})$  is first translated into the triple  $(\eta, \zeta, \omega)$ . This triple is then used to calculate the desired steering angles  $\varphi_i$  and wheel velocities  $v_i$  of the four wheels  $i \in \{1 \dots 4\}$  by solving

$$v_i \begin{pmatrix} \cos \varphi_i \\ \sin \varphi_i \end{pmatrix} = \omega \begin{pmatrix} \cos \zeta \cos \eta - \kappa_G y_{Ri} \sin \zeta \\ \cos \zeta \sin \eta + \kappa_G x_{Ri} \sin \zeta \end{pmatrix}, \quad (11)$$

where  $(x_{Ri}, y_{Ri})$  are the coordinates of wheel  $i$  with respect to the platform center point. For translational motions,  $|\omega|$  is equal to the translational velocity  $|\dot{\mathbf{x}}|$ ; for rotational motions,  $|\kappa_G \omega|$  is equal to the angular velocity  $|\dot{\psi}|$ . Finally, the desired steering angles and wheel velocities are implemented by the local controllers in each wheel-module. A more in-depth description of the mobile platform control can be found in [11].

### 4.3. Position Optimization of the Mobile Platform

The core idea of the presented mobile haptic interfaces consists in using the mobile platform to position the two haptic interfaces at the optimal position in the environment. The position is optimal when it provides the operator with maximum manipulability at all times. Therefore, a mathematical description has to be derived which calculates the optimal platform position. This optimal position is calculated in the platform coordinate system, i.e. it represents a relative position which can be easily transformed to the desired platform velocity by a linear P-controller. The desired velocity is the control input to the platform controller described in the previous section.

In order to simplify the optimization problem, only the planar degrees of freedom are considered. This is possible because the mobile platform can only perform planar motions, i.e. translations in  $x$ - and  $y$ -direction and rotations around the  $z$ -axis. Furthermore, the planar degrees of freedom are also decoupled in the kinematics of the haptic interfaces (cf. Fig. 3). Consequently, only the joint angles  $q_2$  and  $q_3$  of both arms are needed to compute the optimal relative platform position.

### 4.3.1. Manipulability Measure

When maximizing the manipulability of the haptic interfaces, different types of manipulability and different manipulability measures can be considered. Most importantly, one can distinguish between force manipulability and velocity manipulability. In the former case, the configuration dependent ability to exert forces is measured, whereas in the latter case the ability to generate velocity is described. In a device with serial kinematics such as ViSHaRD7, the force manipulability cannot degenerate. In contrast, the velocity manipulability degenerates close to singular configurations (see [21]). Therefore, the optimization strategy is designed to maximize the velocity manipulability of the haptic interfaces. To this end, a manipulability measure based on a singular value decomposition of the Jacobian is used.

The manipulability of the haptic interfaces is bounded by the maximum joint velocities. The resulting maximum velocities in Cartesian space are computed using the Jacobian  $\mathbf{J}(q_2, q_3)$  of the SCARA part of ViSHaRD7. The smallest singular value  $\sigma_m(q_2, q_3)$  of  $\mathbf{J}(q_2, q_3)$  is commonly used as a measure of manipulability. It describes how fast the end-effector can move in an arbitrary direction without allowing the joint velocities  $(q_2, q_3)$  to leave a unit circle. Therefore, maximizing the smallest singular value  $\sigma_m(q_2, q_3)$  also maximizes the allowable Cartesian velocity of the end-effector.

The Jacobian is defined by:

$$\mathbf{J} = \begin{pmatrix} \frac{\delta x}{\delta q_2} & \frac{\delta x}{\delta q_3} \\ \frac{\delta y}{\delta q_2} & \frac{\delta y}{\delta q_3} \end{pmatrix} = \begin{pmatrix} -l_2 \sin(q_2) - l_3 \sin(q_2 + q_3) & -l_3 \sin(q_2 + q_3) \\ l_2 \cos(q_2) + l_3 \cos(q_2 + q_3) & l_3 \cos(q_2 + q_3) \end{pmatrix}. \quad (12)$$

In order to calculate the maximum Cartesian velocities with respect to the given maximum joint velocities  $\dot{q}_{2,max}, \dot{q}_{3,max}$ , a scaled Jacobian is used:

$$\mathbf{R} = \text{diag}(\dot{q}_{2,max}, \dot{q}_{3,max}), \quad (13)$$

$$\tilde{\mathbf{q}} = \mathbf{R}^{-1} \dot{\mathbf{q}}, \text{ where } \mathbf{q} = (q_2, q_3)^T, \quad (14)$$

$$\mathbf{J} \dot{\mathbf{q}} = (\mathbf{J} \mathbf{R}) \tilde{\mathbf{q}} = \tilde{\mathbf{J}} \tilde{\mathbf{q}}, \quad (15)$$

$$\tilde{\mathbf{J}} = \mathbf{J} \mathbf{R} = \mathbf{J} \begin{pmatrix} \dot{q}_{2,max} & 0 \\ 0 & \dot{q}_{3,max} \end{pmatrix}. \quad (16)$$

The smallest singular value  $\tilde{\sigma}_m(q_2, q_3)$  of the scaled Jacobian  $\tilde{\mathbf{J}}(q_2, q_3)$  is the maximum speed with which the manipulator can move in an arbitrary horizontal direction while the joint velocities stay within the given constraints.

Fig. 8 shows the planar velocity manipulability  $\tilde{\sigma}_m(\mathbf{x})$  of one ViSHaRD7 for all reachable end-effector positions. It is affected by angle  $q_3$ , only. Thus, the manipulability is constant on circles around joint 2 and the maximum manipulability is given on a circle with  $r_{opt} = 42$  cm.

### 4.3.2. Maximizing Manipulability

As shown in the previous section, the manipulability is optimal when the end-effector position is located on a circle with radius  $r_{opt}$ . This criterion yields a solution for the optimal angle  $q_3$  of both haptic interfaces.  $q_{r2}$  and  $q_{l2}$  should be chosen in such a way that their

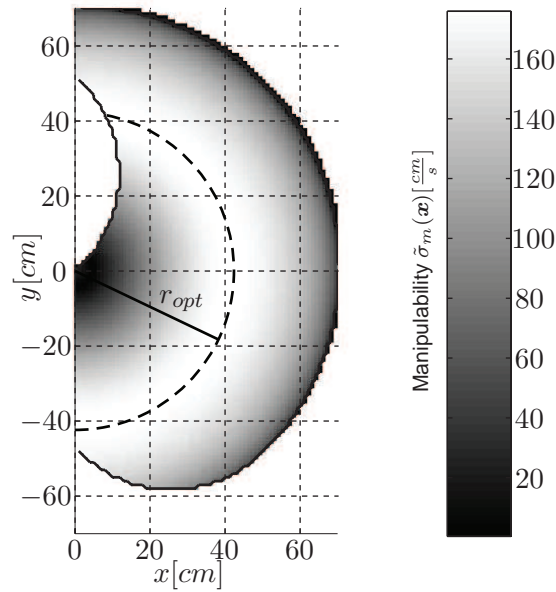


Figure 8. Manipulability and circle with maximum manipulability in the base coordinate system of ViSHaRD7. On the dashed circle the manipulability  $\tilde{\sigma}_m(\mathbf{x})$  is maximized.

minimum distance to the joint limits is maximized. This is achieved when both joint angles,  $q_{r2}$  and  $q_{l2}$ , are equal. The resulting configuration is symmetric and the corresponding platform position can be obtained by simple geometric calculations: the platform must be aligned parallel to the connecting line from  $x_L$  to  $x_R$  and its center point must lie on the perpendicular bisector of the connecting line (see Fig. 9).

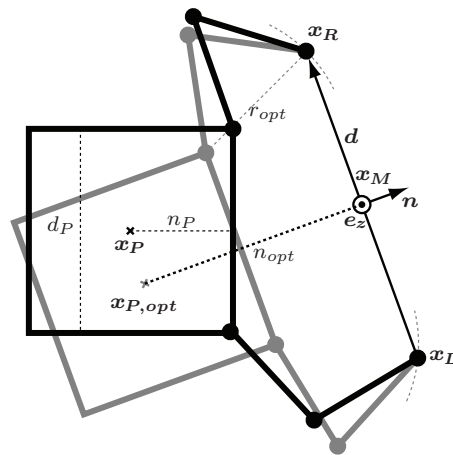


Figure 9. Geometric solution for optimal platform positioning.

The end-effector positions  $x_L$  and  $x_R$  are used to compute the connecting vector  $d$  and

midpoint  $\mathbf{x}_M$ :

$$\mathbf{d} = \mathbf{x}_R - \mathbf{x}_L, \quad (17)$$

$$\mathbf{x}_M = \frac{\mathbf{x}_R + \mathbf{x}_L}{2}. \quad (18)$$

The vector from the optimal platform position  $\mathbf{x}_{P,opt}$  to the midpoint  $\mathbf{x}_M$  is obtained by calculating its direction which is perpendicular to  $\mathbf{d}$  pointing away from the platform and the optimal distance  $n_{opt}$ :

$$\mathbf{n} = \frac{\mathbf{d}}{\|\mathbf{d}\|} \times \mathbf{e}_z \quad (19)$$

$$n_{opt} = \sqrt{r_{opt}^2 - \left(\frac{\|\mathbf{d}\| - d_P}{2}\right)^2} + n_P \quad (20)$$

Finally, the optimal platform position  $\mathbf{x}_{P,opt}$  is calculated:

$$\mathbf{x}_{P,opt} = \mathbf{x}_M - n_{opt} \cdot \mathbf{n} \quad (21)$$

As the platform can only perform planar motions, the  $z$ -component of  $\mathbf{x}_{P,opt}$  is ignored. The optimal platform orientation  $\psi_{P,opt}$  is identical to the direction of the normal vector  $\mathbf{n}$ :

$$\psi_{P,opt} = \angle \mathbf{n} \quad (22)$$

### 4.3.3. Including Human Arm Workspace in Optimization Strategy

The approach presented in the previous section always converges to a configuration of the haptic interfaces which provides the operator with the maximum velocity manipulability. This solution works well for slow motions of the operator where the dynamics of the platform can be neglected. In this case, the end-effector positions will always be close to the points of optimal manipulability. For fast operator motions, however, the mobile platform cannot reposition the haptic interfaces fast enough to avoid a significant degradation of the manipulability. For even faster motions, the end-effectors can reach the boundaries of the admissible workspace.

It is, therefore, desirable to take the different dynamics of human motions into consideration. Analogously to the motions of the mobile haptic interface, human motions can be decomposed into fast motions of limited range which are performed by using the arms only and slower, but unlimited motions performed by using the legs. According to this idea, the mobile platform should always be positioned in such a way that the current workspace of the human arms is mostly covered by the workspace of the two haptic interfaces. This optimization goal requires maximizing the overlap between the workspaces of the human arms and the haptic interfaces. However, this optimization problem cannot be solved in real-time due to its high complexity. Furthermore, the human arms can generate velocities far higher than the maximum velocities of the haptic interface in almost any configuration. But then, only moderate velocities are used in typical application scenarios of the mobile haptic interface.

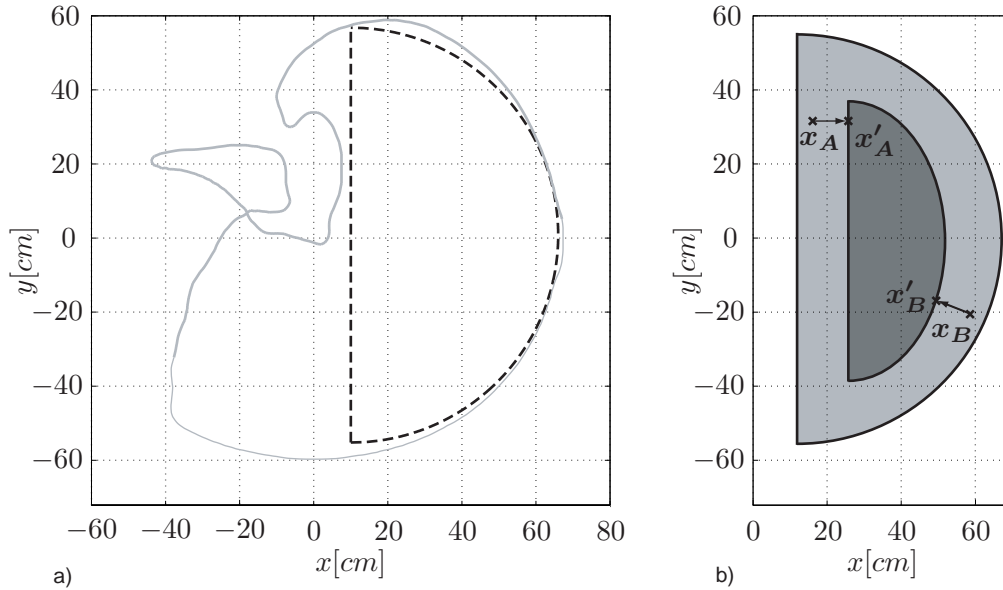


Figure 10. a) Workspace of human right arm in shoulder height (solid line) and approximation by a semicircle (dashed line) b) Mapping from actual to effective end-effector positions. The point of origin is coincident with the shoulder of the human arm.

Therefore, a simplified approach to take the human workspace into account is presented. Fig. 10a shows the computed workspace of the human arm based on a physiological model (see [7]). The relevant workspace can be well approximated by a semicircle.

If the operator holds the end-effectors close to the workspace boundaries of his/her own arm, the respective haptic interface does not need to provide the full motion range in the direction of this boundary. To this end, the position optimization described in Sec. 4.3.2. is no longer applied to the actual end-effector positions  $x_L$  and  $x_R$ , but instead to shifted end-effector positions  $x'_L$  and  $x'_R$ . The method for obtaining these effective end-effector positions is illustrated in Fig. 10b: end-effector positions in the outer region (light-gray) are moved to the border of the inner region (dark-gray). In the inner region, no change is applied.

The advantages of this approach can be seen in figure 11: In condition a), the operator holds the end-effectors close to his/her body. Consequently, his/her arms can only perform small position changes away from the mobile platform, but large position changes in direction of the mobile platform. To account for this asymmetry, the mobile platform is positioned farther away from the end-effectors (cf.  $x_A \rightarrow x'_A$  in Fig.10b). Condition c) shows the opposite condition, where the operator arms are fully extended and the haptic interface is positioned closer to the end-effectors (cf.  $x_B \rightarrow x'_B$  in Fig.10b). Condition b) represents the nominal case without position mapping.

Including the human arm workspace in the position optimization strategy offers advantages when the operator often makes fast motions using the full workspace of his/her arms. However, if the operator performs abrupt motions using his legs, the performance can in some cases be deteriorated because the haptic interfaces are used closer to the workspace

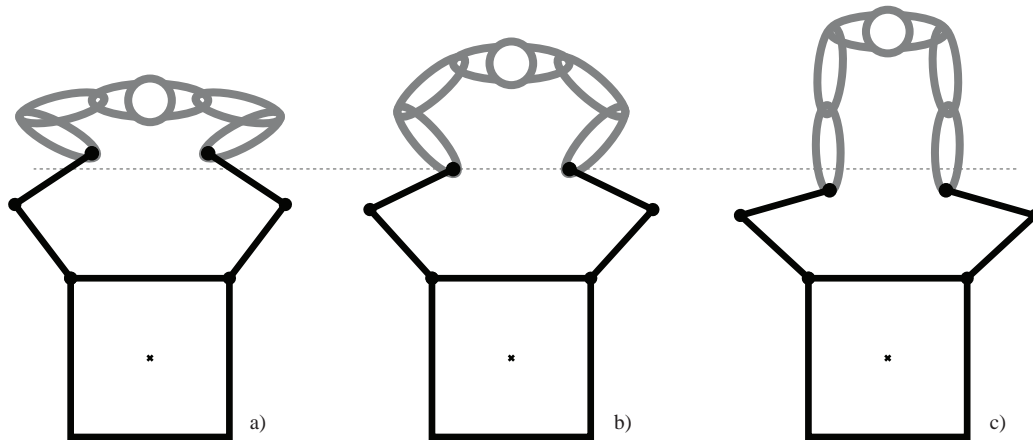


Figure 11. Mobile platform positioning for different arm postures: a) bent arms, b) neutral position, c) extended arms.

limits. Furthermore, it should be noted that including the human arm workspace requires the position of the operator to be tracked. In most application scenarios, the additional effort can be neglected because the position of the operator is already needed to correctly position the teleoperator or avatar.

#### 4.4. Overall Control Structure

The complete control structure of the mobile haptic interface is illustrated in Fig. 12. The interaction forces with the operator are measured for both hands by force/torque-sensors. The controllers of the two haptic interfaces implement the desired master dynamics using an admittance control structure. The resulting end-effector positions are transformed to the platform coordinate system and used to calculate the optimal platform position. The actual end-effector positions  $x_R$ ,  $x_L$  are transformed to account for limitations of the workspace of the human operator as described in the above subsection. From these effective end-effector positions  $x'_R$ ,  $x'_L$  the optimal platform position  $x_{P,opt}$  is determined through simple geometric calculations. The desired optimal platform position is transformed to a desired velocity by employing a linear P-controller, and some non-linear conditioning elements like a small dead-band zone and a velocity and acceleration limiter. Finally, the desired velocity  $\dot{x}_{P,opt}$  is input to the platform velocity controller.

## 5. Experimental Validation

In this section experiments are described which have been conducted in order to validate the designed system. The mobile haptic interface is employed in tasks like exploring large environments, performing local manipulation, carrying objects over large distances, etc.

The evaluation is conducted using a virtual reality (VR). The evaluation task is to move an object along a predefined path which is presented in the VR. The trajectory is chosen such that it includes straight walking, arcs with different curvature, and a zigzag course

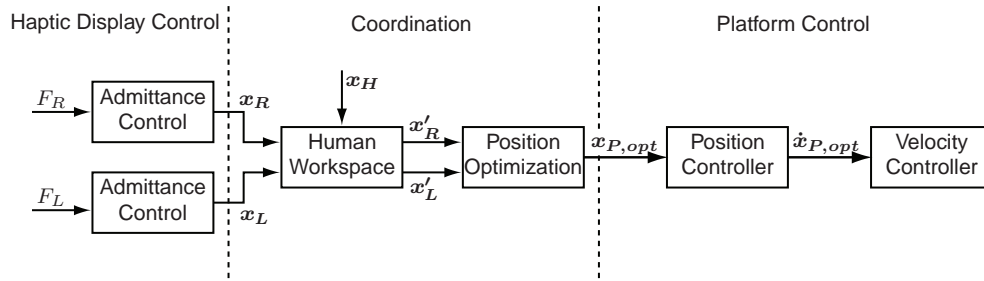


Figure 12. Overall control structure of the mobile haptic interface.

resulting in abrupt changes of the walking direction. This experiment is well suited for assessing the maneuverability of the mobile haptic interface.

### 5.1. Setup

The experiments require an extensive virtual environment in which the operator moves using the mobile haptic interface. Therefore, they are conducted in a laboratory environment of approx.  $5\text{ m} \times 5\text{ m}$  which is fully covered by an acoustic tracking system allowing to record motions of operator and mobile haptic interface. The resolution of the tracking system is about 1 mm. The operator wears a head mounted display (HMD) which gives visual feedback according to the current operator position and gaze direction. The scene is displayed with a resolution of  $1280 \times 1024$  pixel at a framerate of 30 Hz. The visual rendering of the virtual environment is performed on the onboard computers of the mobile haptic interface. This reduces the cabling effort.

The virtual room only contains some structured walls which the operator needs to orient himself/herself and a structured floor with the desired trajectory (see Fig. 13).

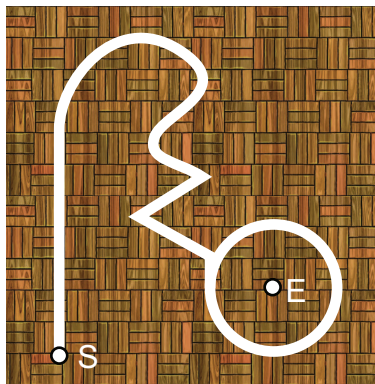


Figure 13. Floor of virtual room with commanded trajectory.

The test persons are instructed to move along the path starting from point  $S$  as fast and accurately as possible. During the movement on the circle, the object must be orientated to the end point  $E$ , resulting in a sideways movement of the test person. The experiment is carried out with persons without any prior experience in the use of haptic interfaces as well as with persons who are acquainted with the use of haptic devices.

## 5.2. Results

During the experiment the travelled path of the operator is recorded in VR coordinates. Two exemplary trajectories taken from an unexperienced and an experienced user are shown in Fig. 14. Obviously, there is a significant training effect in using the mobile haptic interface.

The total travelled distance is 21.2 m for the unexperienced subject and 16.0 m for the experienced subject. The difference is caused by the smaller path deviations and the smaller circle radius for the experienced user. The task execution times for walking along the path are 74 s and 81 s, respectively. The observed results are in accordance with the general experience that operators who are used to employing haptic interfaces tend to operate more slowly but also more precisely. The resulting average speed is between 0.2 m/s and 0.29 m/s which is equivalent to speeds up to a quarter of normal walking speed. As ratios of execution times between telepresent and direct task execution are typically above 10:1, this ratio of 4:1 is comparatively low.

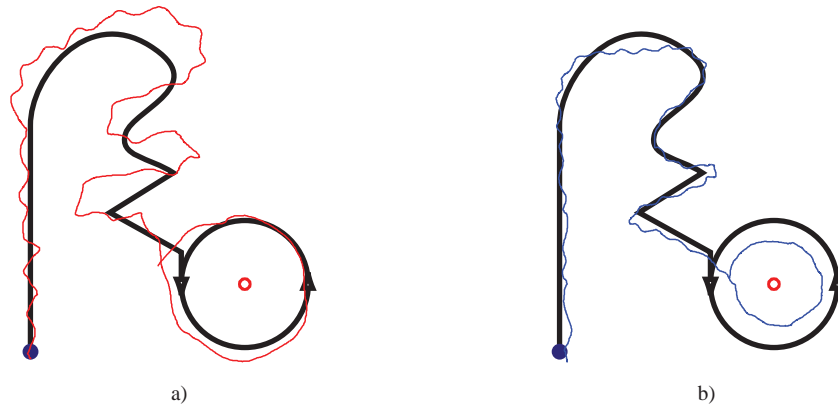


Figure 14. Travelled trajectory: a) unexperienced subject, b) experienced subject.

## 6. Conclusion

A mobile haptic interface allowing simultaneous haptic interaction and natural locomotion in arbitrarily large remote or virtual environments has been presented. The device combines the ability to operate bimanually in full six degrees-of-freedom, high interaction forces and torques, and the useability in extensive scenarios. While devices exist which also provide a solution to one of the mentioned criteria, no other system has been previously presented in the literature which integrates all these aspects into a single device.

For this mobile haptic interface a modular design concept consisting of two different main components - two haptic interfaces and a mobile platform - has been proposed. While the haptic interfaces only cover parts of the human arm workspace, the mobile platform extends these to arbitrarily large remote environments. The presented design and control concepts of the haptic interfaces enable a decoupling of translational from rotational movements, which significantly simplifies the control algorithms which handle the interaction between haptic interfaces and mobile platform. In order to ensure a good manipulability of the haptic interfaces the mobile platform has to be positioned appropriately. Two different optimization strategies to position the mobile platform have been investigated: While the

first approach, based on the maximization of the manipulability of the two haptic interfaces, is suitable only for slow motions of the human operator, the second approach also includes the human workspace in the optimization strategy and thus can also be used for fast operator motions. The experimental results clearly show the good maneuverability of the developed system.

Future research challenges are a more detailed evaluation of the mobile haptic interface and the integration into a teleoperation scenario.

### Acknowledgments

This work is supported in part by the German Research Foundation (DFG) within the collaborative research center SFB453 "High-Fidelity Telepresence and Teleaction. Special thanks go to J. Gradl, H. Kubick, T. Lowitz, and T. Stoeber for their excellent work during the robot construction phase.

### References

- [1] ACROE and Laboratoire ICA. Ergos. (2006). <http://www-acroe.imag.fr/ergos-technologies/>.
- [2] Caldwell, D.G., Wardle, A., Kocak, O., & Goodwin, M. (1996). Telepresence Feedback and Input Systems for a Twin Armed Mobile Robot. *IEEE Robotics & Automation Magazine*, **3**:29–38.
- [3] Darken, R.P. (1999). Spatial orientation and wayfinding in large-scale virtual spaces ii. *Presence*, **8**(6):3–6.
- [4] Formaglio, A., Giannitrapani, A., Franzini, M., Prattichizzo, D., & Barbagli, F. (2005). Performance of mobile haptic interfaces. In *44th IEEE European Control Conference on Decision and Control (CDC-ECC '05)*:8343–8348.
- [5] Grange, S., Conti, F., Rouiller, P., Helmer, P., & Baur, C. (2001). Overview of the Delta Haptic Device. In *Eurohaptics*.
- [6] Hanebeck, U.D., & Saldic, N. (1999). A modular wheel system for mobile robot applications. In *Proceedings of the IEEE/RSJ International Conference on Intelligent Robots and Systems (IROS)*:17–23.
- [7] Klopčar, N., & Lenarčič, J. (2005). *Kinematic Model for Determination of Human Arm Reachable Workspace*. Jozef Stefan Institut, Ljubljana, Slovenien.
- [8] Lee, D., Martinez-Palafox, O., & Spong, M.W. (2006). Bilateral Teleoperation of a Wheeled Mobile Robot over Delayed Communication Network. In *Proceedings of the 2006 IEEE International Conference on Robotics and Automation*, Orlando, Florida.
- [9] Massie, T., & Salisbury, J. (1994). The PHANTOM haptic interface: A device for probing virtual objects. In *Proceedings ASME Winter Annual Meeting: Dynamic Systems and Control Division*, **55**:295–301.

- 
- [10] Nitzsche, N., Hanebeck, U., & Schmidt, G. (2003). Design issues of mobile haptic interfaces. *Journal of Robotic Systems*, **20**(9):549–556.
- [11] Nitzsche, N., & Schmidt, G. (2004). A Mobile Haptic Interface Mastering a Mobile Teleoperator. In *Proceedings of the IEEE/RSJ International Conference on Intelligent Robots and Systems IROS*, Sendai, Japan.
- [12] de Pascale, M., Formaglio, A., & Prattichizzo, D. (2006). A mobile platform for haptic grasping in large environments. *Virtual Reality Journal*, **10**:11–23.
- [13] Peer, A., Komoguchi, Y., & Buss, M. Towards a Mobile Haptic Interface for Bimanual Manipulations. (2007). In *Proceedings of the IEEE/RSJ International Conference on Intelligent Robots and Systems*, submitted.
- [14] Peer, A., Unterhinninghofen, U., & Buss, M. (2006). Tele-assembly in Wide Remote Environments. In *2nd International Workshop on Human-Centered Robotic Systems*, Munich, Germany.
- [15] Quanser Inc. MirageF3D35. (2006). [http://www.quanser.com/english/downloads/products/Specialty/Mirage\\_PIS\\_060806.pdf](http://www.quanser.com/english/downloads/products/Specialty/Mirage_PIS_060806.pdf).
- [16] Schiele, A., & Visentin, G. (2003). The esa human arm exoskeleton for space robotics. In *7th International Symposium on Artificial Intelligence, Robotics and Automation in Space*, Nara, Japan.
- [17] Ueberle, M., & Buss, M. (2004). Control of kinesthetic haptic interfaces. In *Proc. IEEE/RSJ International Conference on Intelligent Robots and Systems, Workshop on Touch and Haptics*.
- [18] Ueberle, M., Mock, N., & Buss, M. (2007). Design, control, and evaluation of a hyper-redundant haptic interface. In M. Ferre, M. Buss, R. Aracil, C. Melchiorri, & C. Balaguer (Eds.), *Advances in Telerobotics: Human System Interfaces, Control, and Applications*. Springer, STAR series.
- [19] Ueberle, M., Mock, N., Peer, A., Michas, C., & Buss, M. (2004). Design and Control Concepts of a Hyper Redundant Haptic Interface for Interaction with Virtual Environments. In *Proceedings of the IEEE/RSJ International Conference on Intelligent Robots and Systems IROS, Workshop on Touch and Haptics*, Sendai, Japan.
- [20] Van der Linde, R.Q., Lammertse, P., Frederiksen, E., & Ruiters, B. (2002). The HapticMaster, a new high-performance haptic interface. In *Eurohaptics'02*:1–5.
- [21] Wen, J.T.-Y., & Wilfinger, L.S. (1999). Kinematic manipulability of general constrained rigid multibody systems. *IEEE Transactions on Robotics and Automation*, **15**(3):558 – 567.